IET Microwaves, Antennas & Propagation

WILEY

The Institution of Engineering and Technology

ORIGINAL RESEARCH OPEN ACCESS

An Octave-Band Orthomode Transducer Design Incorporating Either T-Junctions or Magic-Ts: Performance Comparison and Manufacturing Aspects

Nasrin Tasouji[1] | Sara Salem Hesari[1,2] | Doug Henke[2] | Dave Atherton[2] | Ivan Wevers[2] | Adam Densmore[2] | Jens Bornemann[1]

[1]Department of Electrical and Computer Engineering, University of Victoria, Victoria, British Columbia, Canada | [2]NRC Herzberg Astronomy and Astrophysics Research Centre, Victoria, British Columbia, Canada

Correspondence: Nasrin Tasouji (nasrintasouji@uvic.ca)

Received: 12 November 2025 | **Revised:** 2 February 2026 | **Accepted:** 5 March 2026

Keywords: radio telescopes | waveguide components | waveguide junctions

ABSTRACT

This paper presents an octave-band orthomode transducer (OMT) based on ridged waveguide technology, designed and analysed with both T-junction and Magic-T configurations for performance comparison. The results demonstrate that the Magic-T junction provides superior performance, owing to its inherent characteristics, and outperforms conventional T- and Y-junctions commonly employed for signal recombination in OMTs. The proposed OMT, integrated with a Magic-T and fabricated using CNC machining, achieves octave-band operation from 20 to 40 GHz (2:1). This design addresses fabrication and wideband performance challenges by minimising the number of layers required for CNC machining and by identifying an optimal approach for integrating ridged waveguides throughout the overall OMT structure. The measurement results confirm the OMT's suitability for wideband applications and demonstrate its potential for possible future integration into the next-generation Very Large Array (ngVLA) radio telescope.

1 | Introduction

Orthomode transducers (OMTs) play a crucial role in distinguishing between two orthogonal polarisations, enabling the detection of both circular and linear polarisations in dual-polarised signals. They are essential in various applications, including radio astronomy, where precise polarisation discrimination is critical [1, 2, 3]; radar systems, where they enable separate transmission and reception of orthogonal polarisations for tracking purposes [4, 5, 6]; and satellite communications, in which one polarisation is assigned to the uplink and the other to the downlink, resulting in increased overall traffic capacity [7, 8, 9]. In radio astronomy applications, there is an increasing need to enhance the bandwidth of OMTs to efficiently feed wideband horn antennas. At the same time, enhancing the overall performance of OMTs enables higher levels of waveguide integration within applications such as focal plane array architectures [10]. Broader bandwidths can be achieved by employing ridged waveguides within two folded symmetric configurations, a common approach in wideband OMT designs such as the turnstile junction OMT [11]. Optimising the OMT design directly impacts the noise characteristics of the radio telescope system by addressing challenges such as isolation, spikes, higher-order mode excitation and trapped modes. However, factors such as path length imbalances, asymmetry and fabrication misalignments can degrade the OMT's performance, thus negatively affecting the cross-polarisation characteristics of feed horn antennas [12]. Turnstile OMTs commonly employ Y-junction and T-junction power combiners configured for 180° out-of-phase operation. These combiners recombine the RF signals split by the turnstile junction and route them through waveguide outputs in opposite directions. Although they are simple to design, they suffer from poor isolation between output ports and impedance mismatches. As a result, signal reflections and unwanted coupling can degrade system efficiency and stability, impacting the overall performance of the OMT [13]. Hybrid Magic-T junctions provide a more viable alternative to traditional waveguide junctions in OMTs. Magic-Ts provide excellent port isolation, and the integration of matching features within the Magic-T can further extend the operational bandwidth. A four-port Magic-T network is inherently lossless, reciprocal and impedance-matched at all ports, as it combines the properties of E-plane and H-plane T-junctions [14]. When incorporated into an OMT design, the Magic-T suppresses RF cross-polarisation leakage and exhibits lower sensitivity to manufacturing tolerances [15, 16, 17]. Widely used in focal plane arrays [18], branching networks in communication systems [19], comparator networks [20] and satellite feed clusters [21], Magic-Ts effectively suppress asymmetric modes and spikes. This paper presents the design and development of a waveguide octave-band orthomode transducer (OMT), fabricated in only three layers, for wideband radio receivers. The OMT is tailored to meet the demanding requirements of radio astronomy, with potential application for the next-generation Very Large Array (ngVLA). The demonstrated bandwidth spans 20–40 GHz, fully covering ngVLA Band 4 and partially Band 5. Compared to previously reported OMTs in Refs. [12, 22, 23], the proposed design offers significant improvements in both bandwidth and number of machined layers. The authors in Ref. [12] report a standard 1.66:1 bandwidth, whereas this design achieves full octave coverage. In Ref. [22], the design operates at mm-wave frequencies but uses the conventional T-junction such that it cannot reliably prevent performance degradation from misalignments or resonant spikes. Similarly, the OMT in Ref. [23] is fabricated in six layers, where fabrication errors can lead to spikes, higher-order mode excitation and trapped modes. Two designs are proposed, both incorporating the same turnstile junction and bends but differing in their recombination methods: one using a T-junction and the other a Magic-T. A comparative analysis reveals that the Magic-T configuration exhibits enhanced tolerance to fabrication imperfections compared to the OMT integrated with a T-junction. Given these advantages, the Magic-T-based OMT was selected for fabrication using CNC machining. Additionally, a compact quad-ridged to standard WRD-180 double-ridge waveguide stepped transition was designed, analysed and fabricated. This transition facilitates accurate measurements and enables separate characterisation of each polarisation. This work presents a Magic-T-integrated ridged-waveguide OMT achieving octave-band, spike-free performance, validated by measurements and CNC-machined only in three layers. These specifications distinguish it from existing turnstile OMTs in this frequency band.

2 | Design and Analysis of OMT Components

This section presents the design methodology of the octave-band OMT. The proposed structure incorporates E-bends, H-bends, junctions and a turnstile junction. Accordingly, each element was modelled and optimised individually within the design process to enable efficient optimisation prior to full OMT integration. To reduce insertion loss, the lengths of the waveguide sections, especially the bent waveguides, are optimised to be as short as possible, consistent with the technique used in Ref. [24]. The OMT is designed to operate over 20–40 GHz, with a targeted input reflection coefficient below −20 dB, high port-to-port isolation and low cross-polarisation. Its performance has been validated through full-wave simulations using CST Studio Suite.

2.1 | Turnstile Junction and Ridged Bends

The turnstile junction and bends are designed to operate across the 20–40-GHz bandwidth, achieving a relative bandwidth of 66.66%. Conventional rectangular waveguides cannot support octave bandwidth; therefore, ridged waveguide ports are employed to enhance mode propagation and extend the operational range. Figure 1a–c illustrates the design and simulation results of the turnstile junction, as well as the H-plane and E-plane bends. The reflection coefficients remain below −30 dB across the entire bandwidth, ensuring minimal signal reflection and efficient performance for OMT design. The vacuum is represented by a transparent grey colour, and the ridges are depicted as golden metal.

2.2 | T-Junction and Magic-T Design Comparison

This section compares two ridged waveguide designs and their performance for use as a power combiner in the OMT. Figure 2a depicts a waveguide T-junction functioning as a combining/dividing element. However, as shown in Figure 2b, simulations reveal a critical drawback: The T-junction fails to maintain consistent impedance matching across all ports (i.e., S11 shows excellent input matching, but S22 and S33 are mismatched). Furthermore, the design exhibits inadequate isolation between output ports (approximately −6 dB), limiting its effectiveness in radio astronomy applications, as low isolation adds to signal leakage between output ports.

Alternatively, Figure 3 presents a novel Magic-T design, a hybrid waveguide structure that combines E-plane and H-plane tees and simulated S-parameters. Port 4 functions as the sum port (Σ), whereas Port 1 functions as the E-plane or difference port (Δ). To enhance the bandwidth performance, the Magic-T incorporates internal matching components consisting of ridges and capacitive posts within the H-plane section, integrated with inductive posts in the E-plane arm. Ports 2, 3 and 4 employ single-ridged waveguide configurations, whereas Port 1 utilises a double-ridged WRD180 waveguide to provide compatibility with the standard interface. A stepped rectangular post positioned at the midpoint of the junction near the E-plane output plays a critical role in achieving the required impedance characteristics for Port 1. To facilitate CNC fabrication, this stepped section is directly connected to the entrance of the difference waveguide port and $\pm 50\ \mu$m tolerance is considered for CNC machining of this section. Furthermore, an L-shaped septum is integrated within the sum arm to effectively separate the RF fields and ensure the required isolation between the ports (see Figure 3a). When a signal is applied to the H-plane port, it divides equally between Ports 2 and 3 with identical phase. Conversely, excitation through the E-plane port also results in an equal power split but with a 180° phase difference between the outputs at Ports 2 and 3. Both designs exhibit a reflection coefficient better than −30 dB at Port 1. The Magic-T

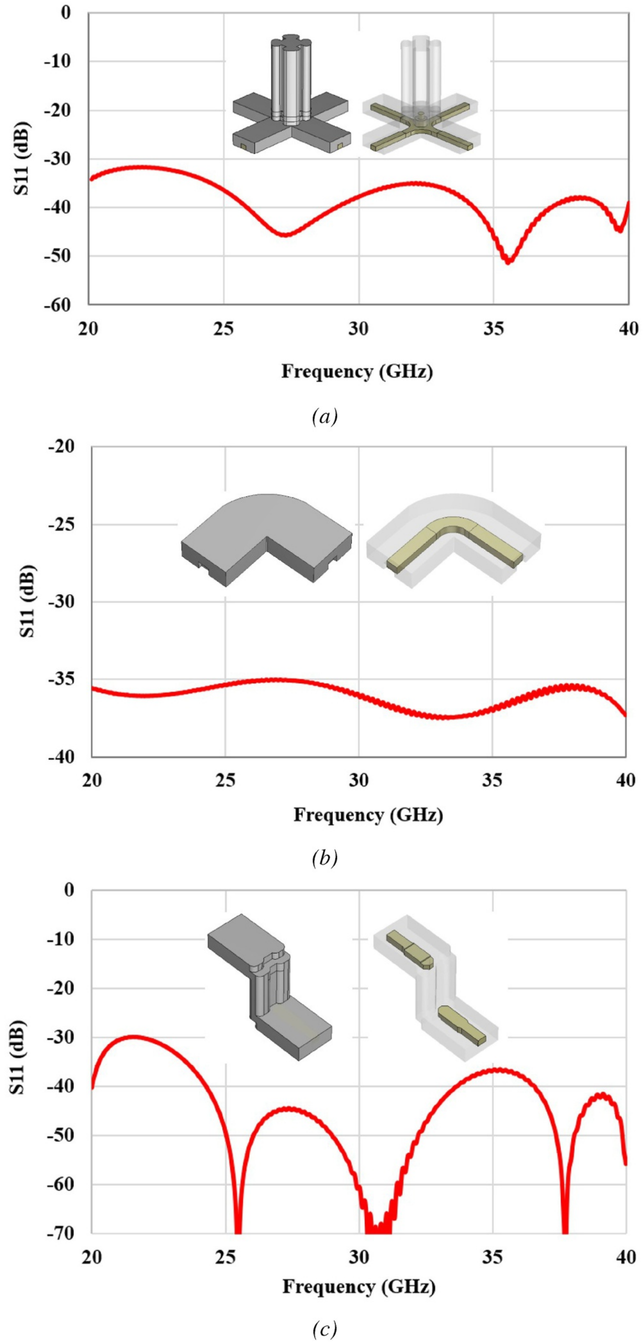

FIGURE 1 | CAD view and simulated reflection coefficient for the (a) quad-ridged waveguide turnstile junction, (b) H-plane bend and (c) E-plane bend.

maintains good performance at Ports 2 and 3, with a reflection coefficient better than − 20 dB, whereas in the T-junction design at these ports it degrades to approximately − 6 dB. In addition, the isolation between Ports 2 and 3 is about − 20 dB for the Magic-T junction, whereas it is only around − 6 dB for the T-junction. See Figures 2b and 3b.

2.3 | Ridged Waveguide Termination

Structural asymmetry or misalignment in an OMT's structure may cause undesirable reflections at the input port, degrading

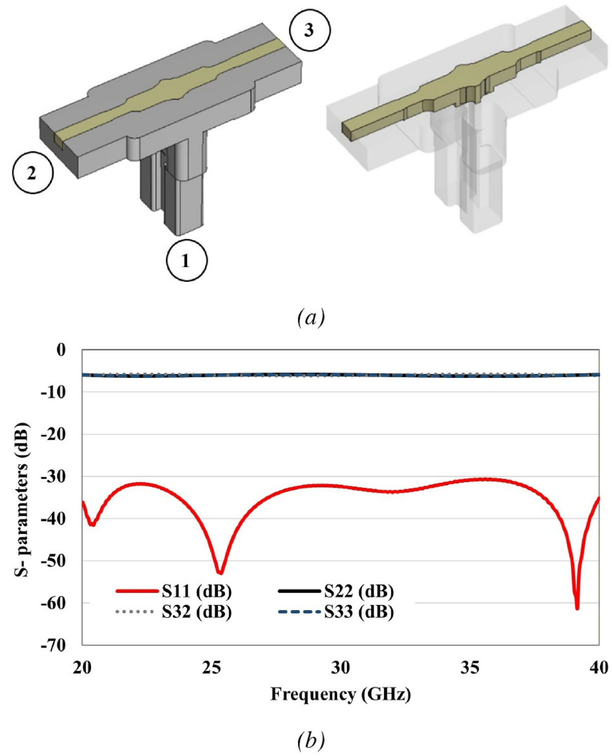

FIGURE 2 | (a) Geometry of the proposed ridged waveguide T-junction, (b) simulated S-parameters of the T-junction.

the overall performance of the OMT. In contrast, the Magic-T structure provides a more effective solution for mitigating these reflections. Any even-mode energy generated due to structural imperfections is directed to the sum port (Σ) in the Magic-T, where it can be terminated. This approach has been successfully implemented in Refs. [12, 17, 21, 25]. Figure 4 illustrates the design details and simulation results of the waveguide termination using Eccosorb MF-117 absorber material, with the electric permittivity assumed to be around 38.

2.4 | Circular Quad-Ridge to Standard Rectangular Double-Ridge WRD-180 Transition

To independently measure each polarisation of the proposed octave-band OMT, a transition from the multimode quad-ridged waveguide to a standard, single-mode double-ridged waveguide is essential. This transition is necessary because the designed quad-ridged waveguide is incompatible with conventional measurement equipment. To address this, a connection to the commercially available WRD-180, a standard double-ridge waveguide-to-coaxial adaptor, is designed. The primary objective in designing this transition was to create a compact structure that could be CNC-machined as a single piece. The transition features a linear step configuration leading to the WRD-180 waveguide and has a precise length optimised for performance. This design achieves a reflection coefficient better than −35 dB while maintaining a higher-order-mode reflection coefficient lower than −80 dB, which is essential for accurate measurement of cross-polarisation leakage and to prevent the formation of trapped modes when the OMT is connected to the horn antenna. A visual depiction of the transition and its

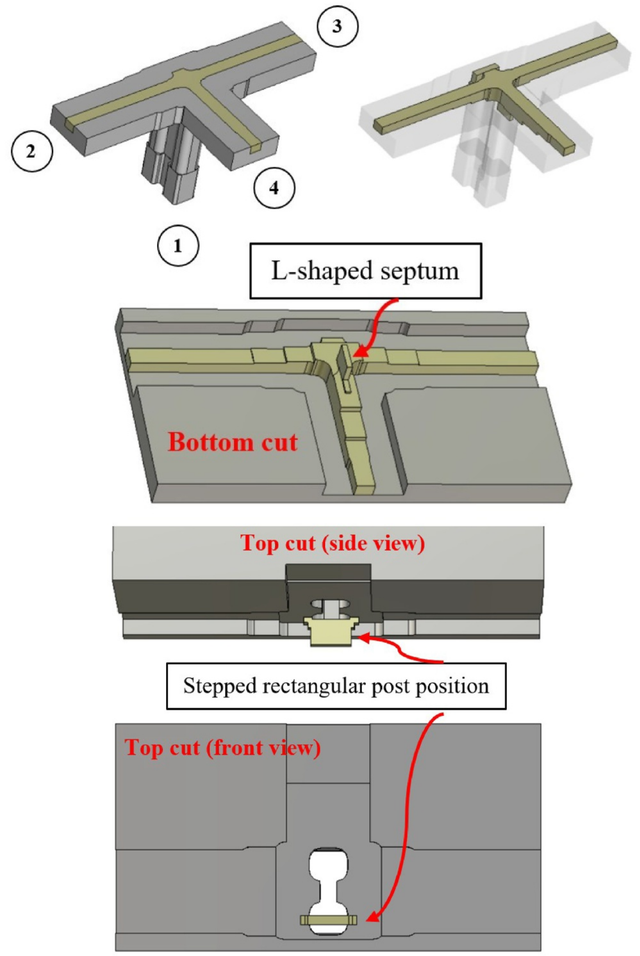

(a)

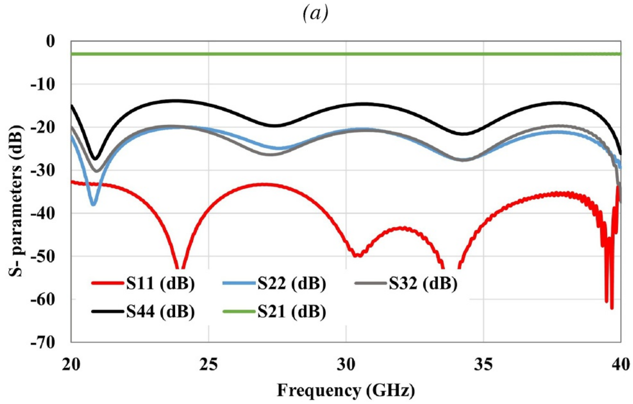

(b)

FIGURE 3 | (a) Geometry of the proposed ridged waveguide Magic-T in full view and two sectional cuts with all internal details, (b) simulated S-parameters of the Magic-T.

corresponding S-parameters is presented in Figure 5a. The measured performance of the OMT is particularly influenced by this transition's quality and mode purity. One effective way to validate the transition for measurement purposes is to connect two identical transitions in a back-to-back configuration [26]. Figure 5b illustrates the back-to-back assembly and simulated S-parameters.

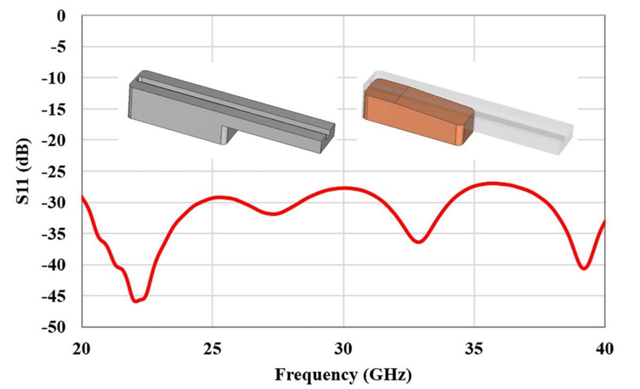

FIGURE 4 | MF-117 waveguide load schematic and simulated reflection coefficient.

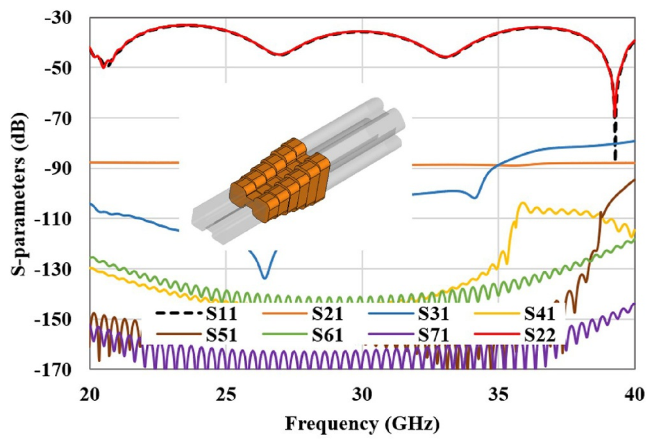

(a)

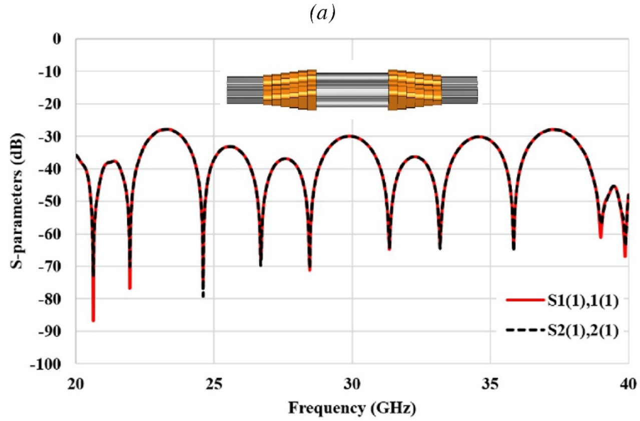

(b)

FIGURE 5 | (a) The transition waveguide cross-section and reflection coefficient and higher-order modes of the transition, assuming perfect alignment, (b) assembly of the transition in a back-to-back configuration and simulated S-parameter results of back-to-back ridged waveguide transitions.

3 | Performance Comparison of OMT Configurations

In this section, the overall OMT configuration is introduced. The OMT is first integrated with the previously described T-junction and then with the proposed Magic-T. An intentional structural asymmetry, denoted by Δ, is then introduced into both configurations. The values of $\Delta = 0$, 0.1, 0.2, 0.3, 0.4 and 0.5 mm are considered to investigate the resulting variations in the S-parameters as the asymmetry increases. This analysis demonstrates the robust performance of the proposed Magic-T and its impact on the overall OMT performance under asymmetric conditions.

3.1 | OMT Integrated With T-Junction

The proposed OMT, with all subcomponents integrated through a T-junction, was simulated in CST Studio Suite for performance comparison. In this configuration, asymmetry is introduced into the OMT arms by deliberately increasing the length of one half of each branch of the OMT by Δ, as shown in Figure 6a. This structural modification disrupts the symmetric recombination of fields within the T-junction, forming trapped modes. These trapped modes are highly undesirable, as they contribute to increased spikes in insertion loss, reflection coefficient, cross-pol and isolation level in the OMT, as illustrated in Figure 6b–e.

3.2 | OMT Integrated With Magic-T Junction

The second design follows the same procedure with the same Δ value; however, the recombination section is a Magic-T, with its fourth arm (sum port) terminated by the dielectric absorber MF-117 (Figure 4). In this configuration, trapped modes are effectively suppressed as any in-phase recombination is coupled into and dissipated by the terminated arm (Figure 7). In contrast to Section 3.2, Figure 7 shows that the simulation results remain spike-free across the full octave band. Furthermore, the excitation of higher-order modes remains low. This makes the design highly suitable for future feed array applications.

4 | Validation and Experimental Results

Considering the simulation results of Sections 3.1 and 3.2, it is evident that the OMT with the Magic-T junction has better performance, considering the possible misalignments and asymmetries that may be caused by fabrication errors. Therefore, the second design was selected as the final design for fabrication. Figure 8 indicates the equivalent circuit of the OMT. All machining was completed by NRC's Design and Fabrication Services (DFS), Victoria, BC (Figure 9). The OMT components were machined with high precision, maintaining tolerances within $\pm 10\ \mu$m. The fabrication process often requires multiple iterations, as any dimensional deviation typically necessitates the remanufacturing of the component. The environment in which the parts are machined is maintained at a constant 20.5 °C to ensure dimensional stability. In addition, any raw stock to be machined, as well as measuring tools, must be in the climate-controlled room for a period of at least 24 h in advance of use to ensure that they have thermally stabilised to the controlled temperature. The size of the part features necessitates comparably small cutting tools, and surface finish is important for

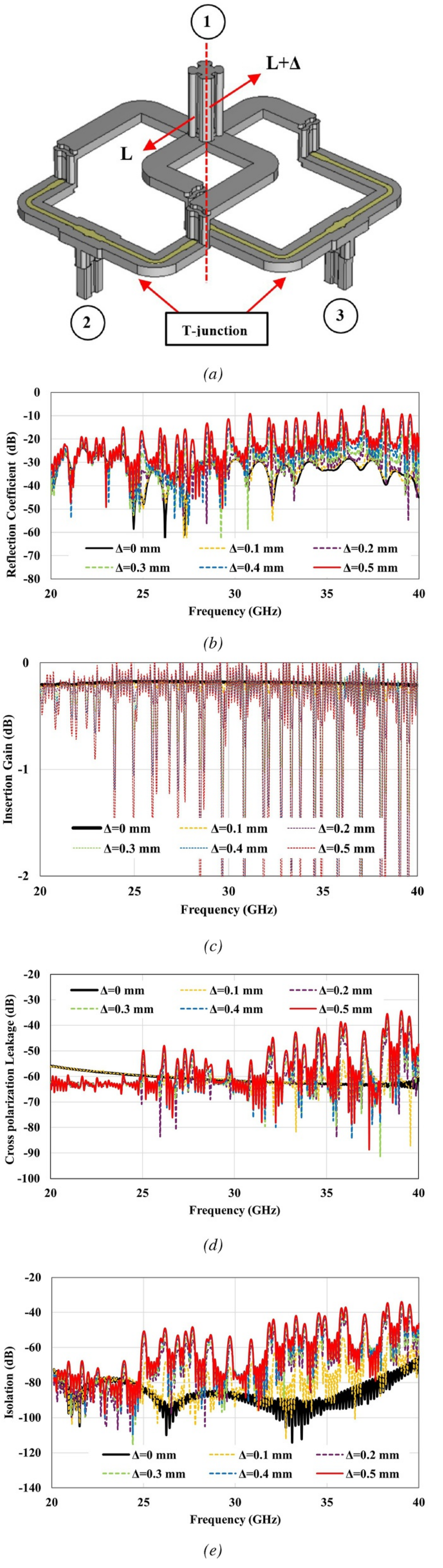

FIGURE 6 | (a) Geometry of the proposed ridged waveguide OMT using a T-junction as combiner, (b) simulated reflection coefficient for Port 1, (c) insertion loss, (d) simulated cross-polarisation and (e) simulated isolation of the symmetric and asymmetric OMT.

performance. A prototype of the turnstile-junction OMT was fabricated based on the optimised dimensions obtained from CST simulations while accounting for practical fabrication

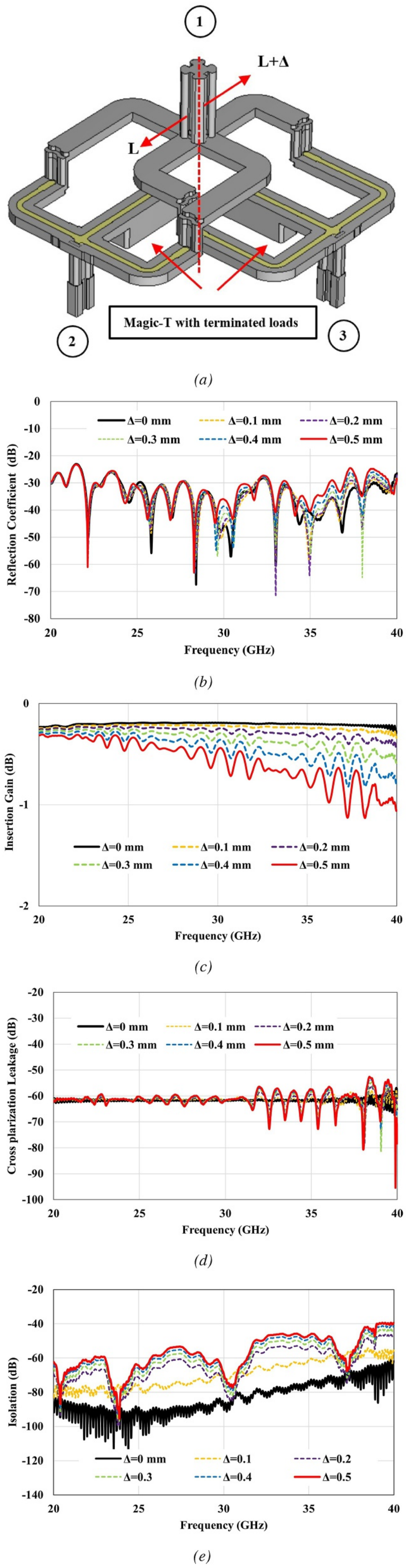

FIGURE 7 | (a) Geometry of the proposed ridged waveguide OMT using Magic-T as combiner, (b) simulated reflection coefficient for Port 1, (c) insertion loss, (d) simulated cross-polarisation and (e) simulated isolation of the symmetric and asymmetric OMT.

constraints. The OMT fabrication material is aluminium 6063-T6 with an electrical conductivity of 53 (% IACS), approximately 2×10^7 S/m. Figure 10a,b shows photographs of the

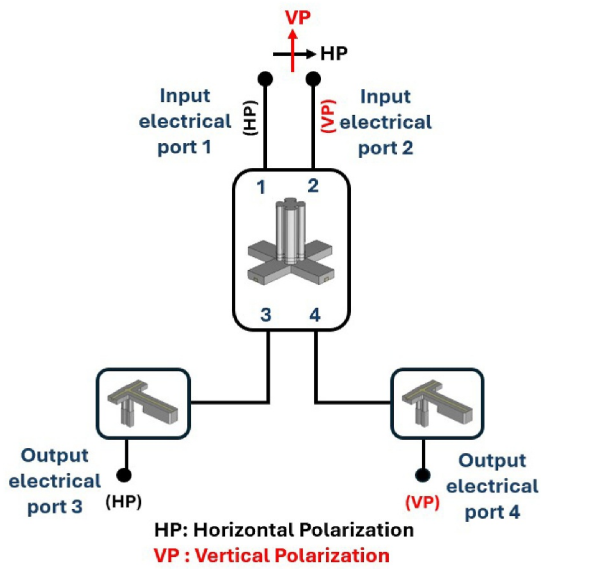

FIGURE 8 | Principal equivalent circuit of the proposed OMT.

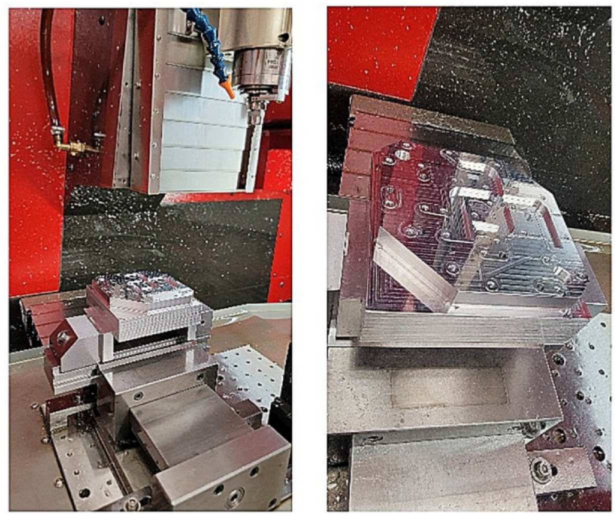

FIGURE 9 | OMT machining in progress at the DFS facility at NRC Herzberg.

OMT fabricated in three layers, and Figure 10c shows the OMT connected to the designed quad-ridged circular waveguide-to-double-ridged standard rectangular WRD-180 waveguide transition. Figure 10d shows the standard rectangular WRD-180 double-ridged waveguide-to-coax adaptor used for connection to the vector network analyser.

The prototype was measured using a Keysight PNA N5227B vector network analyser, and it is calibrated using a waveguide SOLT-type calibration with a WRD180 calibration kit, employing a Thru, a fixed matched load and two offset short standards of different electrical lengths. The offset shorts provide the necessary phase reference to characterise reflection errors, whereas the load improves match accuracy, and Thru establishes the measurement reference planes at the waveguide flanges. The measured versus simulated results are presented in Figure 11. The measured reflection coefficient for the common circular ridged waveguide is almost −20 dB across most of the

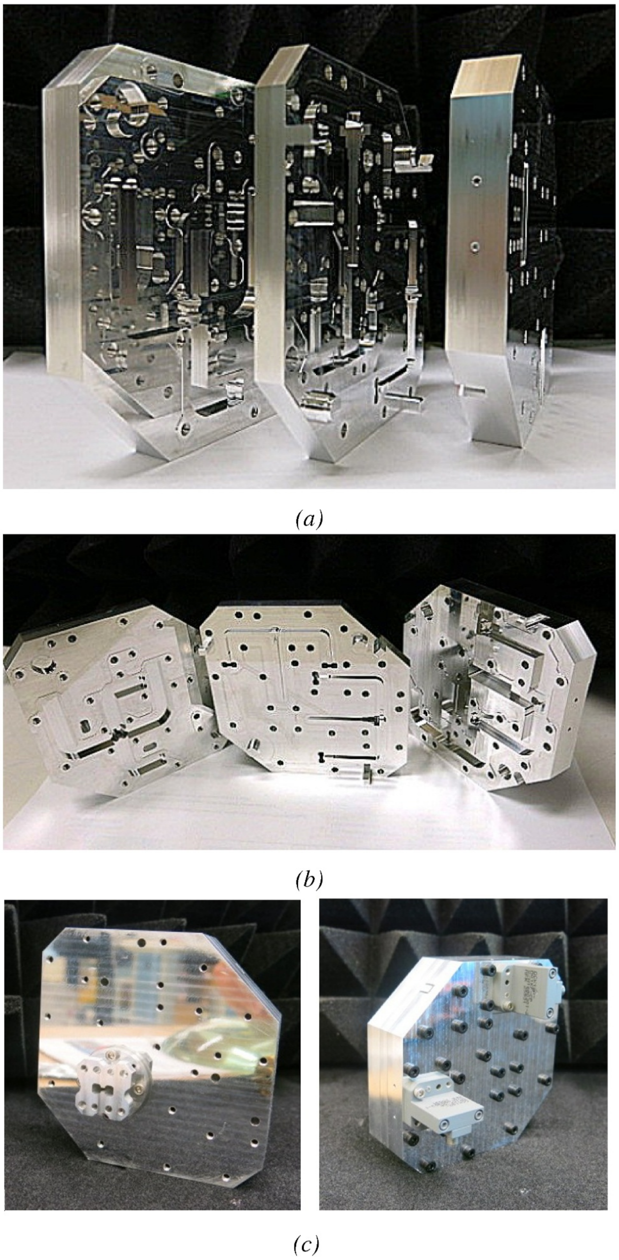

FIGURE 10 | (a) Disassembled view of the OMT layers, (b) detailed view of the OMT split-block, (c) transition coupled to the OMT input waveguide (left) and OMT outputs connected to a standard WRD-180 waveguide (right).

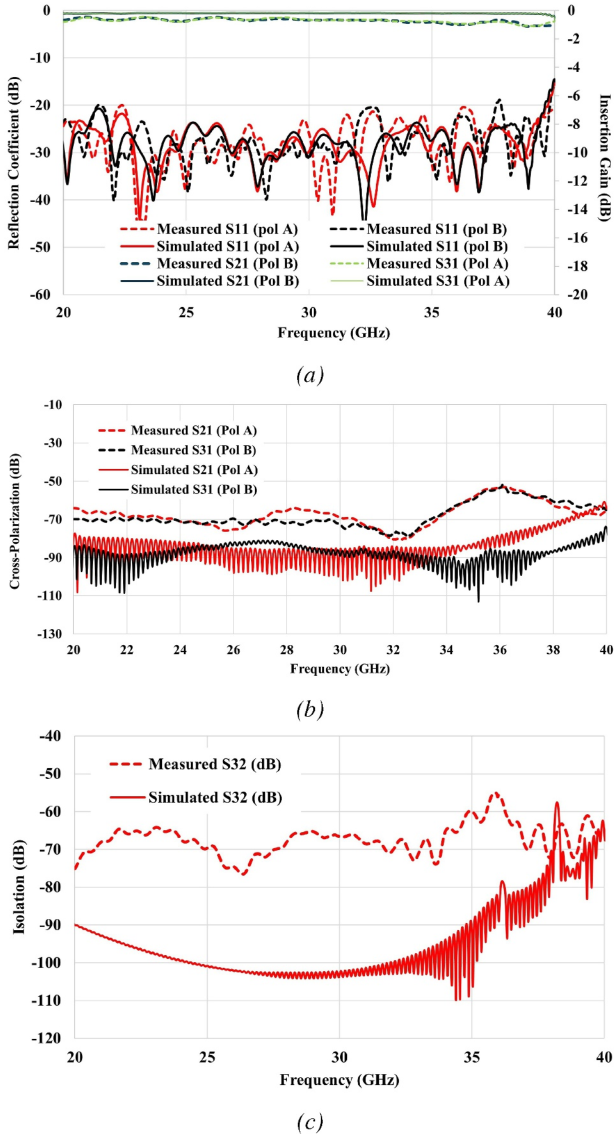

FIGURE 11 | Measured versus simulated: (a) reflection coefficients and insertion loss, (b) cross-polarisation and (c) isolation of the fabricated OMT when it is connected to the transition.

frequency band, cross-polarisation leakage is better than almost −60 dB, insertion loss is approximately around 0.7 dB, and isolation between the two double-ridged output waveguides is better than almost −60 dB over the frequency range from 20 to 40 GHz. The discrepancy between the simulated and measured results can be attributed to any possible assembly misalignments and measurement setup limitations. Table 1 compares the proposed turnstile-junction OMT with previously reported designs in terms of measured performance, fabrication technology and the number of machined layers. The proposed OMT achieves a wider bandwidth while requiring fewer machined layers, and it demonstrates superior S-parameter performance, which clearly distinguishes it from earlier turnstile-junction OMT implementations.

5 | Conclusion

Two prototypes of turnstile-junction OMTs were designed based on a T-junction and a Magic-T configuration, with a detailed performance comparison demonstrating that the Magic-T-based design yields superior results. The Magic-T-based OMT was fabricated and experimentally characterised to enable polarisation multiplexing and enhance bandwidth efficiency in antenna systems. Measured results demonstrate the OMT's inherent potential for radio astronomy and communication systems applications, considering its octave-band bandwidth, substantially fewer trapped modes and lower spikes compared

TABLE 1 | Comparison of mmW turnstile OMTs.

Reference	Frequency range (GHz)	FBW (%)	Return loss (dB) Max (avg.)	Insertion loss (dB) (Avg.)	Isolation (dB) (Avg.)	Cross-polarisation (dB) (Avg.)	Fabrication technology
[12]	30.5–50.5	49.4	22	0.45	50	48	CNC milling (3 layers)
[23]	24–51	72	16	0.3	60	60	CNC milling (6 layers)
[27]	13.5–18.1	29	25	0.05	—	55	CNC milling (5 layers)
[28]	67–116	54	20	4.5	30	30	CNC milling (4 layers)
[29]	220–330	40	20	0.3	—	50	Silicon micromachining
[30]	75–110	38	17/15	0.5/0.6	28	—	3-D printed
[31]	29–50	53	20	0.5/1.6	50	50	CNC milling (3 layers)
This work	20–40	66.7	20	0.7	60	60	CNC milling (3 layers)

to earlier turnstile-junction OMTs, confirming its enhanced performance in practical applications.

Author Contributions

Nasrin Tasouji: conceptualization, data curation, formal analysis, investigation, methodology, software, validation, visualization, writing – original draft. **Sara Salem Hesari:** conceptualization, funding acquisition, investigation, methodology, project administration, resources, software, supervision, validation, writing – review and editing. **Doug Henke:** conceptualization, investigation, methodology, resources, software, supervision, validation, writing – review and editing. **Dave Atherton:** resources, validation, writing – review and editing. **Ivan Wevers:** software, visualization, writing – review and editing. **Adam Densmore:** resources, writing – review and editing. **Jens Bornemann:** conceptualization, funding acquisition, investigation, methodology, project administration, resources, software, supervision, validation, writing – review and editing.

Acknowledgements

The authors wish to express their appreciation to NRC's Design and Fabrication Services (DFS), Victoria, BC, for their valuable assistance in the fabrication of the prototype components.

Funding

The authors have nothing to report.

Conflicts of Interest

The authors declare no conflicts of interest.

Data Availability Statement

Data are available upon request from the authors.

References

1. A. Gonzalez and K. Kaneko, "High-Performance Wideband Double-Ridged Waveguide OMT for the 275–500 GHz Band," *IEEE Transactions on Terahertz Science and Technology* 11, no. 3 (May 2021): 345–350, https://doi.org/10.1109/TTHZ.2021.3062451.

2. D. W. Henke, N. Jiang, S. S. Hesari, A. Seyfollahi, B. Veidt, and L. B. G. Knee, "Octave Bandwidth Receiver Technology for Radio and Millimetre-Wave Telescopes," in *Proceedings SPIE 12190, Millimeter, Submillimeter, and Far-Infrared Detectors and Instrumentation for Astronomy XI*, (2022): 121901Y, https://doi.org/10.1117/12.2630537.

3. S. Salem Hesari, D. Henke, V. Reshetov, et al., "Design and Analysis of the NRC Q-Band Receiver for ngVLA Band-5," *Proceedings of SPIE* 12190 (August 2022): 310–329, https://doi.org/10.1117/12.2627870.

4. C. A. Leal-Sevillano, K. B. Cooper, E. Decrossas, et al., "Compact Duplexing for a 680-GHz Radar Using a Waveguide Orthomode Transducer," *IEEE Transactions on Microwave Theory and Techniques* 62, no. 11 (November 2014): 2833–2842, https://doi.org/10.1109/TMTT.2014.2359636.

5. M. A. Abdelaal, S. I. Shams, and A. A. Kishk, "Asymmetric Compact OMT for X-Band SAR Applications," *IEEE Transactions on Microwave Theory and Techniques* 66, no. 4 (April 2018): 1856–1863, https://doi.org/10.1109/TMTT.2018.2791960.

6. S.-G. Park, H. Lee, and Y.-H. Kim, "A Turnstile Junction Waveguide Orthomode Transducer for the Simultaneous Dual Polarization Radar," in *Asia Pacific Microwave Conference* (IEEE, 2009), 135–138.

7. A. Tribak, J. L. Cano, A. Mediavilla, and M. Boussouis, "Octave Bandwidth Compact Turnstile-based Orthomode Transducer," *IEEE Microwave and Wireless Components Letters* 20, no. 10 (October 2010): 539–541, https://doi.org/10.1109/LMWC.2010.2060261.

8. A. E. Kamili, A. Tribak, J. Terhzaz, and A. M. Sanchez, "A Dual Band Orthomode Transducer in K/Ka Bands for Satellite Communications Applications," *Progress in Electromagnetics Research Letters* 73 (2018): 77–82, https://doi.org/10.2528/pierl17112202.

9. D. Garcia, V. Cabrera, and J. M. M. Ruiz, "High Performance of Dual band/dual Polarization Compact OMT," in *IEEE-APS Topical Conference on Antennas and Propagation in Wireless Communications (APWC)*, (2013): 703–706, https://doi.org/10.1109/APWC.2013.6624899.

10. D. Henke and C. Groppi, "Focal Plane Array Concept for ALMA 2030," in *ALMA Front End Develop* (Workshop, September 2021), https://doi.org/10.5281/zenodo.5548445.

11. N. Tasouji, S. S. Hesari, D. Henke, et al., *Compact Turnstile quad-ridge Orthomode Transducer with Octave Bandwidth for Radio Astronomy Applications* (International Society for Optics and Photonics, 2024), https://doi.org/10.1117/12.3017641.105

12. D. Henke, D. Atherton, I. Wevers, and A. Densmore, "An Orthomode Transducer (OMT) Using Magic Tees for Improved Performance, Manufacturing, and Integration," *IEEE Transactions on Microwave Theory and Techniques* 73, no. 8 (2025): 5088–5095, https://doi.org/10.1109/TMTT.2025.3530347.

13. J. Uher, J. Bornemann, and U. Rosenberg, *Waveguide Components for Antenna Feed Systems: Theory and CAD* (Artech House, 1993).

14. D. M. Pozar, *Microwave Engineering* (Wiley, 1998).

15. N. J. G. Fonseca, "Compact Waveguide Orthomode Transducer Without Crossings," in *13th International Symposium on Antenna Technology and Applied Electromagnetics (ANTEM/URSI)*, (2009), https://doi.org/10.1109/ANTEMURSI.2009.4805064.

16. B. Hozouri, "Orthomode Transducer," Patent US 2006/0 226 931 A1, (2006).

17. E. Reiche, S. Stirland, C. Hartwanger, U. P. Hong, R. Gehring, and H. Wolf, "A Dual Circular Combined K/Ka-Band RF Sensing Feed Chain for Multi Beam Satellite Antennas," in *5th European Conference on Antennas and Propagation (EUCAP)* (IEEE, 2011), 3198–3202.

18. D. T. Chuss, A. Ali, M. Amiri, et al., "Cosmology Large Angular Scale Surveyor (CLASS) Focal Plane Development," *Journal of Low Temperature Physics* 184, no. 3–4 (August 2016): 759–764, https://doi.org/10.1007/s10909-015-1368-9.

19. E. Reiche, S. Stirland, C. Hartwanger, U. P. Hong, R. Gehring, and H. Wolf, "A Dual Circular Combined K/Ka-Band RF Sensing Feed Chain for Multi Beam Satellite Antennas," in *5th European Conference on Antennas and Propagation (EUCAP)* (IEEE, 2011), 3198–3202.

20. G. L. Huang, S. G. Zhou, and T. H. Chio, "Highly-Efficient Self-Compact Monopulse Antenna System With Integrated Comparator Network for RF Industrial Applications," *IEEE Transactions on Industrial Electronics* 64, no. 1 (January 2017): 674–681, https://doi.org/10.1109/TIE.2016.2608769.

21. G. L. Huang, S. G. Zhou, and T. Yuan, "Design of a Compact Wideband Feed Cluster With Dual-Polarized Sum- and Difference-Patterns Implemented via 3-D Metal Printing," *IEEE Transactions on Industrial Electronics* 65, no. 9 (September 2018): 7353–7362, https://doi.org/10.1109/TIE.2018.2793842.

22. N. Tasouji, S. S. Hesari, D. Henke, and J. Bornemann, "Design of an Ultra Wideband Ridged Waveguide Turnstile Orthomode Transducer for mm-Wave Radio Astronomy Applications," in *IEEE International Symposium on Antennas and Propagation and North American Radio Science Meeting (APS/URSI)*, (July 2025). Paper No.1313.

23. D. Henke, N. Kelly, K. Marshall, I. Wevers, and L. B. G. Knee, "A Turnstile Quad-Ridge Orthomode Transducer (OMT) for Octave-Bandwidth Receiver Front-Ends (24–51 GHz)," *IEEE Transactions on Microwave Theory and Techniques* 71, no. 11 (November 2023): 4906–4921, https://doi.org/10.1109/TMTT.2023.3267544.

24. I. Lapkin, C. D. López, D. Meledin, et al., "Wideband OMT for the 210–373 GHz Band With Built-In 90° Waveguide Twist," *IEEE Transactions on Terahertz Science and Technology* 15, no. 2 (March 2025): 151–157, https://doi.org/10.1109/TTHZ.2024.3499734.

25. S. Sierra-Garcia, Y. Demers, and J. P. Langevin, "High Power PIM-Free Spike-Free Ortho-Mode Transducer," in *European Conference on Antennas and Propagation (EuCAP)*, (2006).

26. M. A. Abdelaal, S. I. Shams, M. A. Moharram, M. Elsaadany, and A. A. Kishk, "Compact Full Band OMT Based on Dual-Mode Double-Ridge Waveguide," *IEEE Transactions on Microwave Theory and Techniques* 66, no. 6 (June 2018): 2767–2774, https://doi.org/10.1109/TMTT.2018.2825402.

27. R. Nesti, E. Orsi, G. Pelosi, and S. Selleri, "Design of Two Ku-Band Orthomode Transducers for Radio Astronomy Applications," *Progress in Electromagnetics Research* 163 (2018): 79–87, https://doi.org/10.2528/PIER18062002.

28. I. Barrueto, N. Reyes, P. Mena, and L. Bronfman, "A Broadband Orthomode Transducer for the New ALMA Band 2+3 (67–116 Ghz)," in *2016 Global Symposium on Millimeter Waves (GSMM) & ESA Workshop on Millimetre-Wave Technology and Applications* (Espoo, Finland, 2016), 1–4, https://doi.org/10.1109/GSMM.2016.7500322.

29. A. Gomez-Torrent, U. Shah, and J. Oberhammer, "Compact Silicon-Micromachined Wideband 220–330-GHz Turnstile Orthomode Transducer," *IEEE Transactions on Terahertz Science and Technology* 9, no. 1 (2019): 38–46, https://doi.org/10.1109/TTHZ.2018.2882745.

30. J. Shen and D. S. Ricketts, "Compact W-Band "Swan Neck" Turnstile Junction Orthomode Transducer Implemented by 3-D Printing," *IEEE Transactions on Microwave Theory and Techniques* 68, no. 8 (August 2020): 3312–3321, https://doi.org/10.1109/TMTT.2020.2992065.

31. C.-C. Chiong, C. Chien, C.-C. Chang, Y. D. Huang, and Y.-J. Hwang, "Cryogenic 29–50 GHz Orthomode Transducer for Radio Astronomical Receiver," in *2018 Asia-Pacific Microwave Conference (APMC)* (IEEE, 2018), 1271–1273, https://doi.org/10.23919/APMC.2018.8617524.